Influence of surface microstructure parameters on wear of steel ball unfolding wheel

C. Y. Pan [a,b,*], J. H. Chang[a,b], G. Q. Cao[a,b]
[a]Key Laboratory of Advanced Manufacturing and Intelligent Technology, Ministry of Education, China
[b]School of Mechanical and Power Engineering, Harbin University of Science and Technology, Harbin, China

The unfolding wheel is an important part of the steel ball tester in rolling bearing industry, and it is easy to be worn out. In this study, the pit microstructure is applied to the working surface of the unfolding wheel to reduce wear, improve its service life and reduce the testing cost of the steel ball. To analyze the influence of surface microstructure geometrical parameters on the abrasion of unfolding wheel under dry friction condition, the following research was conducted. First of all, the influence of shape, area, depth, and spacing of the microstructure pits on the abrasion of the specimen surface is studied by the orthogonal test method. Then, the subsurface stress of microstructure in contact with the steel ball is analyzed by ANSYS software. Comparing the simulated stress distribution with experimental wear mass, it is found that the more concentrated the high-stress area, the less wear. The diamond microstructure with a single pit area of 3.14×10^{-2} mm^2 and a depth of 100 μm has the best abrasion reduction effect. Finally, the mathematical models including microstructure geometrical parameters for calculating the wear mass of microstructure surface are established. The mathematical models can be used to predict the life of steel ball unfolding wheel and assist the design.

1. Introduction

As the rolling body of the bearing, steel ball plays an important role in its performance [1]. In the process of steel ball manufacture, some damage and defects will inevitably occur on the surface. These surface damages and defects can affect the operation of the bearing or even lead to damage of the bearing. Therefore, it is important to measure the surface quality of the steel ball [2-3]. The wear of the unfolding wheel due to friction during the test of the steel ball will affect the measuring accuracy and efficiency, which will lead to the invalidation of it [4-5].

In recent years, improving wear resistance by machining pits, bulges, or stripes on the surface of metal parts, mimicking the microstructure of the surfaces of living organisms, has proved to be very effective [6]. Many scholars have studied methods to improve the friction and wear characteristics of friction pairs based on the theory of bionic tribology [7-10]. Ma et al. analyzed the effects of different experimental factors on the friction coefficient and wear amount of the shells of clams [11], by studying the microscopic morphology and tribological characteristics of the shells of Clam. Hu et al. used a laser to study the effect of the microstructure surface on the friction properties of GCr15 steel [12]. The scanning electron microscope (SEM) was used to observe the wear appearance of the metallographic surface. It was found that the

friction coefficient and wear were lower than that of the smooth surface under dry friction conditions. Otero et al. argue that microstructures increase the likelihood of controlled geometric features on a micron-scale [13], which will affect the mechanisms of fluid lubrication and wear interactions. Jeyaprakash et al. studied the microstructure of the surface of nodular cast iron processed by laser and proved that the hardness and abrasion resistance of the workpiece surface was improved by the laser processing[14]. Tong et al. made an experimental and simulation analysis on wear resistance mechanism and properties of carbide microstructure materials [15]. Wan et al. studied the optimization of tool microstructure parameters [16].

In this paper, the pit microstructure is applied to the working surface of the unfolding wheel to reduce the wear of the wheel, improve its service life and decrease the testing cost of bearing steel balls. The effects of shape, area, depth, and spacing on wear are studied by dry friction experiments and stress simulation, and the optimum microstructure parameters for wear reduction are sought.

2. Experimental methods and analysis

As shown in Fig. 1, the working surface of the unfolding wheel consists of two offset cones with two conical axes on the same plane and at opposite angles α to the unfolding wheel axis, generally $1°$. When working, the ball is subjected to force Q from the driving wheel, which spins around at angular speed ω_1, drives the sphere at an angular speed ω_2 around the z-axis, and steers the unfolding wheel at an angular velocity ω_3. The steel ball is subjected to the normal force F_n and the tangent friction F_f produced by the two tapered surfaces of the unfolding wheel. The tangent friction F_f drives the ball to spin around the x-axis at a slower speed of ω_2'. The function of the unfolding wheel is to rotate the ball around the z-axis as well as the x-axis. A point on the sphere moves in a spiral in space. During the process of detection, all points on it can pass through the inspection probe and play the role of spreading out the full surface [17].
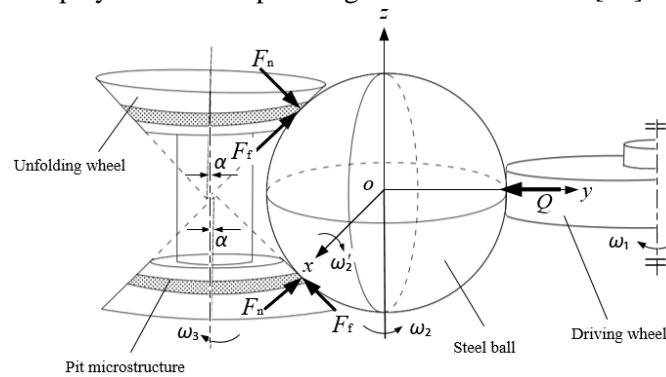

Fig. 1. Working diagram of the unfolding wheel.

2.1. Experimental methods

During the working process, the lateral rotation of the steel ball in *yoz* plane produces the sliding dry friction between the ball and the cone surface, which is easy to cause the opening surface to be worn out. To reduce the wear, the pit microstructure is applied to the contact area between the two cone faces of the expanding wheel and the steel ball. To make the wear experiment more widely applicable, the surface of the unwrapping wheel is expanded and made up

into a flat ring, as shown in Fig. 2. The contact between the steel ball and the cone is replaced by the contact of the ball with the plane. The wear experiments and simulations are simplified by using a cylinder instead of the cone.
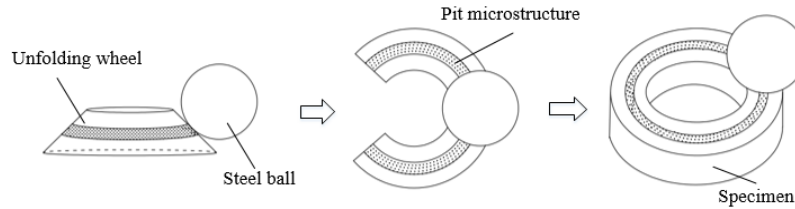

Fig. 2. Model simplification process.

The testing device is shown in Fig. 3(a). A disk-shaped specimen with a concave pit microstructure on the surface is shown in Fig. 3(b). Microstructural shapes are round, square, and diamond which are processed by laser ablation. The specimen is made of Cr1Mo2W50 with internal diameter, external diameter, and height of ϕ28 mm, ϕ54 mm, and 18 mm respectively, as the material of the unfolding wheel. The ball is made of GCr15 steel and has a diameter of ϕ28 mm.
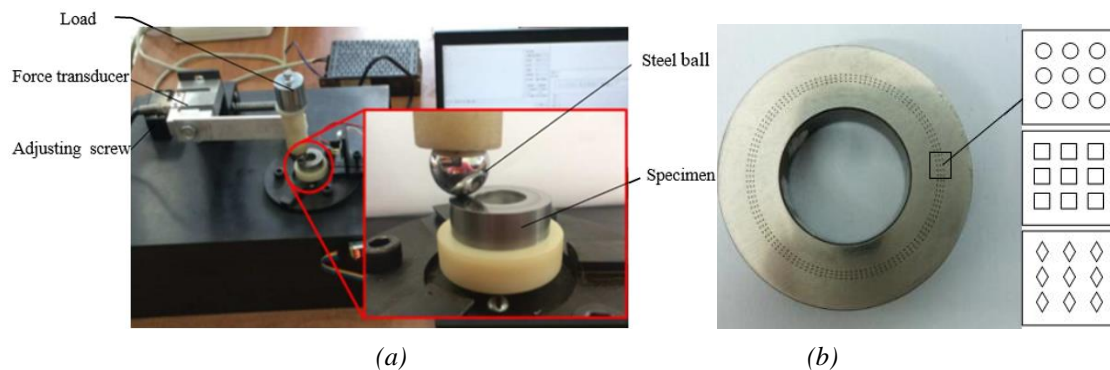

(a)   *(b)*

Fig. 3. The friction wear testing device(a) and specimen(b).

The orthogonal experimental design method was adopted, in which shape (round, square, diamond), area (7.85×10^{-3} mm^2, 1.76×10^{-2} mm^2, 3.14×10^{-2} mm^2) depth (50 μm, 100 μm, 150 μm) and circumferential spacing (2.5°, 3.0°, 3.6°) were used as the experimental factors to carry out the orthogonality experiment on abrasion. The microstructures viewed under super depth of field microscope VHX-1000 were shown in Fig. 4. The experimental load was set to 2N and the wear time to 5 hours. The rotational speed of the sample was 1500 r/min. The wear mass was measured by precise electronic balance BSM 220.4.
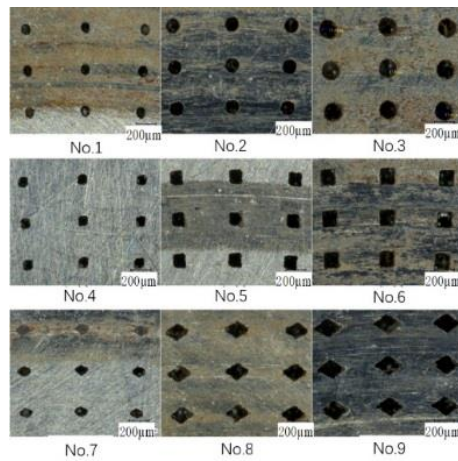
Fig. 4. Microstructure photos of specimens under microscope.

2.2. Experimental results and analysis

The wear mass of different specimens was measured through wear experiments, and the results are listed in the Table 1.

Table 1. Experimental result.

Experiment number	Shape	Area/mm^2	Depth/μm	Spacing / °	Wear mass/mg
1	1(Round)	1(7.85×10^{-3})	1(50)	1（2.5°）	5.6
2	1	2(1.76×10^{-2})	2(100)	2（3.0°）	4.1
3	1	3(3.14×10^{-2})	3(150)	3（3.6°）	3.2
4	2(Square)	1	2	3	4.4
5	2	2	3	1	3.2
6	2	3	1	2	2.9
7	3(Diamond)	1	3	2	4.2
8	3	2	1	3	3.5
9	3	3	2	1	2.2
K_{j1}	12.9	14.2	12.0	11.0	-
K_{j2}	10.5	10.8	10.7	11.2	-
K_{j3}	9.9	8.30	10.6	11.1	-
R_j	1.00	1.96	0.47	0.07	-

In   Table   1, $\overline{K_{j_l}} = K_{j_l}/3, \ R_j = max\left\{\overline{K_{j_1}}, \overline{K_{j_2}}, \overline{K_{j_3}}\right\} - min\left\{\overline{K_{j_1}}, \overline{K_{j_2}}, \overline{K_{j_3}}\right\}$

.

It is shown that the symbol of R_j indicates that the influence of the factor on wear mass is larger. By analyzing the wear experimental data in Table 1, the order of significance of the influence of geometrical parameters of the microstructure is as follows: area > shape > depth > spacing. Moreover, the value of R_j for the spacing is 0. 07, meaning the influence of spacing on wear is too small to be considered.

Because the area and shape of microstructure have an obvious influence on the wear mass of the microsurgical specimen, to intuitively reflect the effect of microstructure area and shape on the wear mass, the experimental results of table 1 are drawn as a line graph, as shown in Fig. 5. Obviously, the wear mass decreases with the increase of pit area in the condition of the shape of the same pit. From table 1 and Fig. 5, it can be found that the least wear mass point is No. 9. That means when the microstructure is diamond, the area is 3.14×10^{-2} mm^2, and the depth is 100 µm, it has a better anti-wear effect.
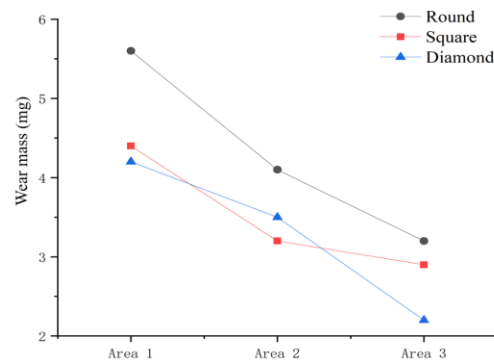

Fig. 5. Effect of area and shape on wear mass.

3. Results and analysis of stress simulation

To further study the wear mechanism of microstructure surface and considering the durability of surface contact, surface stress and subsurface stresses need to be analyzed. According to the above experiment, a three-dimensional simulation model is established, and the stress simulation is analyzed by ANSYS software. The material properties were entered and the model of contact between the steel ball and microstructure surface was established. The specimen material was Cr1Mo2W50, the elastic modulus was 5.32×10^5 MPa and the Poisson ratio was 0.24. The steel ball material is GCr15 with an elastic modulus of 2.07×10^5 MPa and a Poisson ratio of 0.30. The stress analysis of round-shaped microstructure, square-shaped microstructure, and diamond microstructure was carried out with a depth of 100µm and an area of 3.14×10^{-2} mm^2 respectively. The results of the stress simulation are shown in Fig. 6.
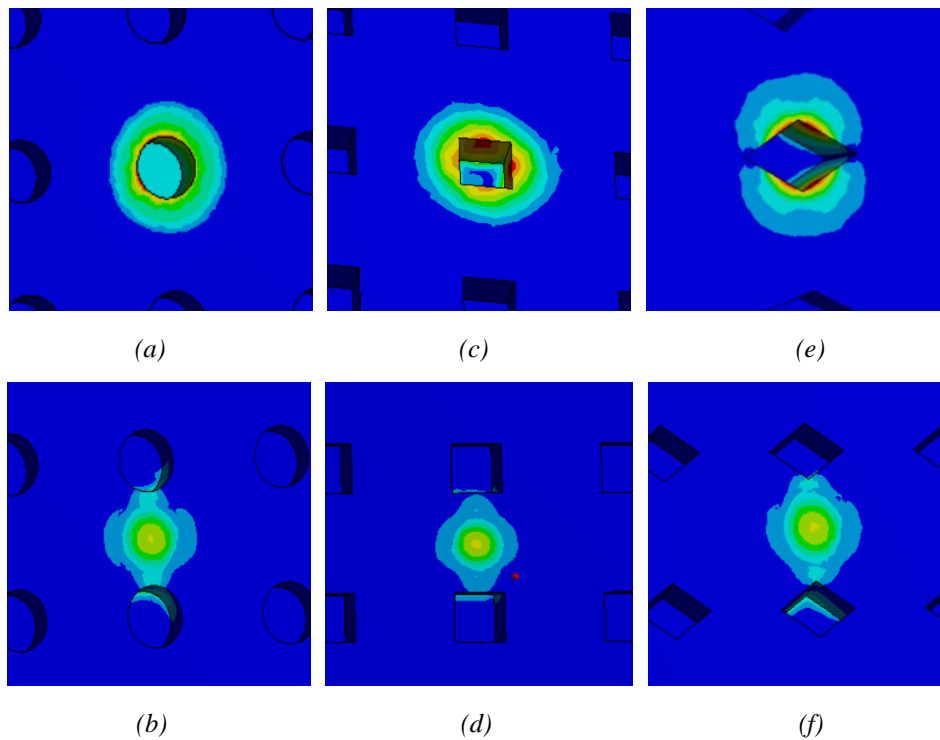
Fig. 6. Stress simulation at different positions on the surface of the microstructure:
(a) (b) Round, (c) (d) Square, (e) (f) Diamond.

It can be seen that when the steel ball is in contact with the pit in the middle, it produces great stress, and the stress acts on the vicinity of one pit, other pits are unaffected. When the steel ball is in contact with the point outside the pit, the stress is small, and it has little effect on the wear. Therefore, only the stress of a single micro-structure crater needs to be analyzed in detail.

3.1. Influence of pit area on stress distribution

To study the influence of pit area on abrasion, circular pits with the same depth of $100\mu m$ but with different size diameters of the small, medium, and large were selected. The micro-structure single pit areas were 7.85×10^{-3} mm^2, 1.76×10^{-2} mm^2, and 3.14×10^{-2} mm^2.

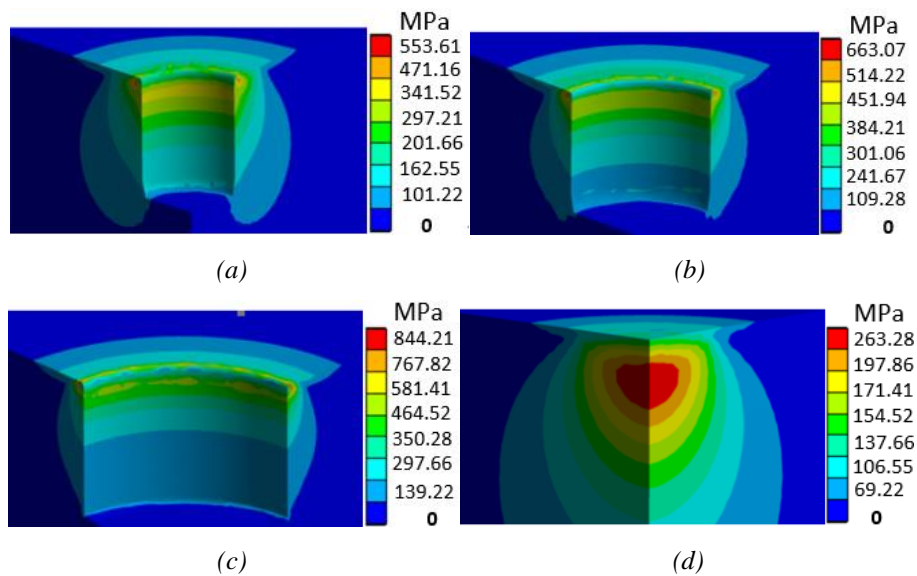*Fig. 7. Stress simulation of different microstructure areas and no microstructure:*
(a) 7.85×10^{-3} mm^2, (b) 1.76×10^{-2} mm^2, (c) 3.14×10^{-2} mm^2, (b) 0 mm^2.

As can be seen from Fig. 7, the larger the area of a single crater of microstructure and the smaller the high-stress area, it is more likely that the high-stress location will be located in a hardened zone near the edge of the craters formed during laser processing. Although the larger the microstructure area, the greater the maximum stress, but the high-stress areas distributed around the microstructure crater, and very close to the surface, in the material hardening zone, so reduce the possibility of fatigue crack and micro-debris flaking. In the absence of microstructure, although the maximum stress is smaller, the high-stress zone is located in the deeper subsurface, and the high-stress area is larger, far from the specimen surface. Therefore, under the action of the deep and extensive secondary surface stress, the surface without microstructure is easy to form the peeling off of large metal particles in the working process, which is to make the abrasion aggravate.

3.2. Influence of pit shape on stress distribution

To study the influence of shape on abrasion, stress simulation was carried out on three microstructures(circular, square, diamond) with the same depth of 100μm and an area of 3.14× 10^{-2} mm^2. The simulation results of square and diamond microstructures are shown in Fig. 8 and the stress distribution of a circular microstructure is illustrated in Fig. 7(c).
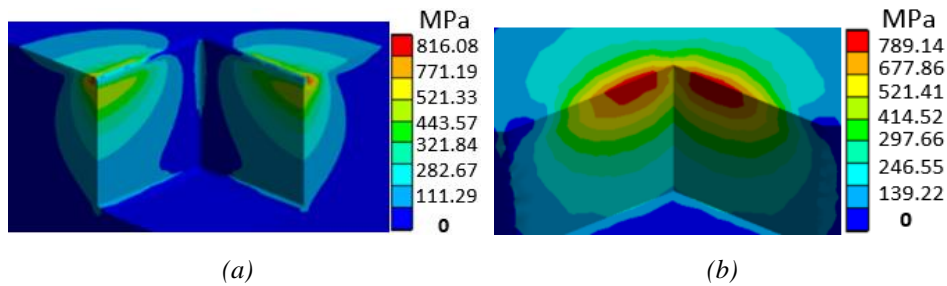
(a)   *(b)*

Fig. 8. Stress simulation of the microstructure of square and diamond: (a) Square, (b) Diamond.

A comparison of Fig. 8 and Fig. 7(c) shows that the maximum stress of diamond microstructures is minimal (789.14 MPa). The maximum stress of the circular microstructure is 844.21 MPa. The maximum stress of the square-shaped microstructure is 816.08 MPa. The difference in the volume of the high-stress area of the three microstructure shapes is not obvious, but the value of maximum stress is different. It can be concluded that the wear of microstructures of different shapes is related to the peak stress under the same pit area. The diamond microstructure has the smallest stress peak and the best wear resistance. The peak stress of the square microstructure is slightly larger than that of the diamond, and its wear resistance is medium. The peak stress of circular microstructure is the largest and the wear resistance is relatively poor.

3.3. Influence of pit depth on stress distribution

To study the influence of depth on abrasion, micro-structures with circular pits and different depth (50 μm、100μm、150 μm) with a same area of 3.14×10^{-2} mm^2 were selected for stress simulation. The results of stress simulation for microstructures of 50 μm and 150 μm depth are shown in Fig. 9. The results of stress simulation for microstructures of 100 μm depth are shown in Fig. 7(c).
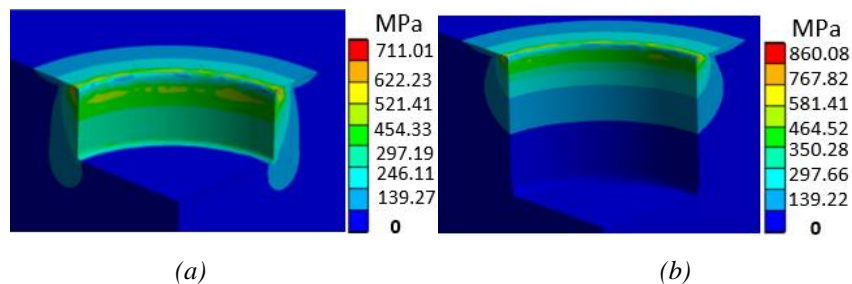

(a)   *(b)*

Fig. 9. Stress simulation of different depths: (a) 50μm, (b) 150μm.

A comparison of Fig. 9 and Fig. 7(c) shows that, while the maximum stress is small (711.01 MPa) at a relatively shallow depth (50 μm), a second stress concentration zone is formed at the bottom of the pit and thus leads to increased wear. When the depth of the pit is 100 μm and 150 μm, the maximum stress is 844.21 MPa and 860.08 MPa, it can be seen that when the pit reaches a certain depth (more than 100 μm), the maximum stress increases slightly and the

variation of stress distribution will not be obvious. It can be concluded that the second stress concentration area is formed at the bottom of the pit when the depth of microstructure is insufficient, and the wear resistance is not the best. With the increase of pit depth, the stress concentration at the bottom of the pit will decrease, and the performance will be improved. When the depth of the pit reaches a certain critical value, the secondary stress concentration area vanishes. At this point, if the depth of the pit continues to increase, it has no obvious effect on the reduction of abrasion.

4. Theoretical analysis

A common model of wear is the Archard wear model [15] in the form shown below.

$$V = K\frac{LP}{H}$$

(1)

In the formula: V is wear volume; K is the wear coefficient. L is the distance of wear; P is the load; H is the material hardness. Wear distance L can be expressed as the product of relative velocity v and time t at the point of contact.

$$L = vt$$

(2)

Take the formula (2) into formula (1) and multiply the two sides of the equation by the material density ρ equals the expression of wear weight:

$$W = \rho K\frac{vtP}{H}$$

(3)

The material hardness H is changed and is difficult to be measured considering the hardening action of machining. The wear coefficient is recorded as K_1 equaling K/H, and the expression is obtained due to deformation of above formula

$$K_1 = K/H$$

(4)

$$W = \rho K_1 vtP$$

(5)

Considering that the surface contact stress distribution of the steel ball and microstructure specimens will change K_1, the microstructure area S, shape coefficient A (A is the ratio of the longest axis to the shortest axis for the geometrical center), and depth h are used to modify K_1. The spacing effect is small and negligible.

Considering the hardness H of the surface material after the machining of microstructure, the probability of grinding grains K produced by the known parameters is directly proportional to K_1, and K is in direct proportion to the volume V and the maximal stress σ in the high-stress region. The influence increases with depth h within a certain range, and the effect decreases with increasing depth beyond this range. At a depth of 0, K_1 should be the same as K/H as measured in the microstructure free test, so the following relationship is assumed:

$$K_1 = a_0 V \sigma \ln(a_1 h + 1) + K_0 \tag{6}$$

In the formula, a_0 and a_1 are unknown constants, and K_0 is the result of K/H measured in the microstructure free test.

According to the simulation results, the volume V of the high-stress region is mainly related to microstructure area $S(\text{mm}^2)$ and depth $h(\mu\text{m})$. Maximum stress σ is also associated with the size S and the shape coefficient A of microstructures, so that the relationship is nonlinear, as shown below.

$$\begin{cases} V = a_2 S^{a_3} h^{a_4} \\ \sigma = a_5 S^{a_6} A^{a_7} \end{cases} \tag{7}$$

In the formula, a_2、a_3、a_4、a_5、a_6、a_7 are unknown constants.

The formula (7) is brought into formula(6) and the constant term is combined to obtain a modified equation for K_1.

$$K_1 = b_0 S^{b_1} A^{b_2} h^{b_3} \ln(b_4 h + 1) + K_0 \tag{8}$$

The K_1 of different microstructures are obtained by taking the experimental data into formula (5) and are listed in Table 2. The relationship between the wear coefficient and the microstructure parameters is given by using the least square fitting method to solve the unknown constants (b_0, b_1, b_2, $b_{3,}$ and b_4) according to the formula (8).

Table 2. K_1 calculated from the test.

Experiment number	K_1	Experiment number	K_1	Experiment number	K_1
1	6.13×10^{-6}	4	4.70×10^{-6}	7	4.70×10^{-6}
2	4.49×10^{-6}	5	3.50×10^{-6}	8	3.94×10^{-6}
3	3.50×10^{-6}	6	3.06×10^{-6}	9	2.52×10^{-6}

$$K_1 = 2.307 \times 10^{-5} - 1.107\, S^{0.0822} A^{0.1019} h^{-0.9283} \ln(1.120 \times 10^{-3}\, h + 1) \tag{9}$$

The fitting advantage parameter of the function in formula (9) is $R^2 = 0.99$, which means that the formula is in good agreement with the experimental data.

The formula for calculating the wear of microstructure unfolding wheels by bringing the formula (9) into formula (5) is as follows：

$$W = \rho\, v\, t\, P(2.307 \times 10^{-5} - 1.107\, S^{0.0822} A^{0.1019} h^{-0.9283} \ln(1.120 \times 10^{-3}\, h + 1) \tag{10}$$

The influence of the depth of microstructure is not obvious from the wear experiment. Therefore, the following wear model is established based on the abrasion formula and considering only the effect of area and shape.

$$K_1^{'} = b_0\, S^{b_1} A^{b_2} + K_0 \tag{11}$$

The least-square method is used to fit formula (11), and the unknown constants b_0, b_1, and b_2 are solved, which are substituted into formula (11).

$$K_1^{'} =- 2.584 \times 10^{-5} S^{0.082} A^{0.102} + 2.307 \times 10^{-5} \tag{12}$$

$$W^{'} = \rho v t P (- 2.584 \times 10^{-5} S^{0.082} A^{0.102} + 2.307 \times 10^{-5}) \tag{13}$$

Input the data of experimental data into formula (10) and (13), calculate the wear and compare the results with experimental wear mass, as shown in Fig. 11. It shows that the wear model of equation (10) considering the influence of shape, area, and depth is similar to the experimental data. The wear model of equation (13) considering only the shape and area are not similar to experimental results in whole, the coinciding points are No.2, No.4, No.5, No.6, and No.9. The mathematical model of equation (10) performs well on the square microstructure. Using the formula (10) to calculate the surface abrasion of microstructure has higher accuracy, with a maximum error of 4.6 %. Therefore, the life of the unfolding wheel can be predicted by using equations (10) and (13). So the design of the microstructure surface unfolding wheel would be assisted.
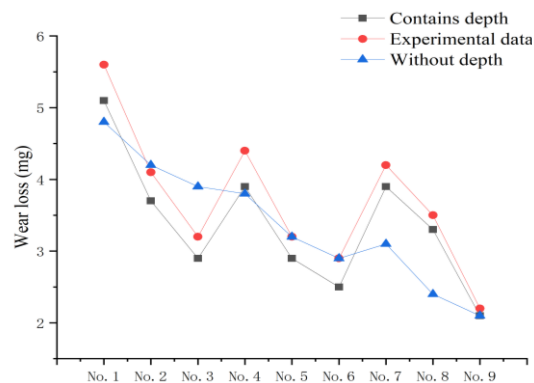

Fig. 10. Comparison of test wear and calculation wear.

5. Conclusion

It is found that the parameters that affect the apparent degree of abrasion are area > shape > depth > spacing. When the microstructure is diamond, the area is 3.14×10^{-2} mm^2, and the depth is 100 μm, it has a better anti-wear effect.

Through stress simulation analysis, it is found that different geometric parameters change the stress distribution of microstructure pits and affect the volume of high-stress zones, which is the root cause of the amount of wear. The amount of wear is reduced when the area of the pit is

increased. The diamond pit is better than the circle and the square ones, and the microstructure depth needs to reach more than 100 μm to achieve a better grinding effect.

The Archard wear model is modified and a wear calculation formula with microstructural parameters (shape coefficient *A*, area *S*, depth *h*) is established, which can be used to predict the life of the microstructure surface unfolding wheel.

Acknowledgments

References

[1] Z. Kai, F. L. Hua, W. Zhong, Optical Engineering **56**(10), 104 (2017).

[2] H. Y. Zhang, L. Y. Ma, F. Q. Xie, Journal of the International Measurement Confederation **144**(192), 7714 (2019).

[3] H. Y. Zhang, F. Q. Xie, M. Y. Cao, Sensors **7**(17), 7 (2017).

[4] Y. L. Zhao, C. T. Xia, H. B. Wang, Chinese Journal of Mechanical Engineering **28**(3), 521 (2015).

[5] C. Y. Pan, X. Li, H. P. Wang, Mechanisms and Machine Science **77**(2), 518 (2020).

[6] S. W. Zhang, Lubrication Engineering **43**(1), 1 (2018).

[7] S. Q. Fang, S. Klein, H. C. Zhang, International Journal of Refractory Metals & Hard Materials **84**(4), 105034 (2019).

[8] P. Lu, R. Wood, G. Mark, Tribology International **113**(1), 169 (2017).

[9] S. G. Ye, H. S. Tang, R. Yan, Applied Mathematical Modelling **77**(1), 554 (2019).

[10] X. H. Zhan, P. Yi, Y. C. Liu, Proceedings of the Institution of Mechanical Engineers Part C-journal of Mechanical Engineering Science **234**(7), 1382 (2020).

[11] Y. H. Ma, F. D. Lin, Z. F. Yan, Transactions of the Chinese Society of Agricultural Engineering (Transactions of the CSAE) **29**(18), 298 (2013).

[12] T. C. Hu, D. Qi, H. L. Tian. Tribology **31**(5), 447 (2011).

[13] N. Otero, P. Romero, A. Gonzalez. Journal of Laser Micro Nenoengineering **7**(2), 152 (2012).

[14] N. Jeyaprakash, C. H. Yang, M. Du, Results in Physics **15**(10), 102585 (2019).

[15] X. Tong, S. C. Su, X. L. Liu, Proceedings of the Institution of Mechanical Engineers part C-journal of Mechanical Engineering Science **233**(17), 5989 (2019).

[16] Q. Wan, M. Zheng, S. Yang, International Journal of Simulation Modelling **18**(3), 543 (2019).

[17] Y. L. Zhao, Z. Q. Zhao, Y. D. Bao, Journal of Mechanical Engineering **52**(17), 205 (2016).